Computation and Evaluation of the Electromagnetic Parameters of Amorphous Core Transformers

Bao Doan Thanh
Faculty of Engineering and Technology, University of Quy Nhon, Vietnam
doanthanhbao@qnu.edu.vn (corresponding author)

Vuong Dang Quoc
School of Electrical and Electronic Engineering, Hanoi University of Science and Technology, Vietnam
vuong.dangquoc@hust.edu.vn

Received: 2 September 2023 | Revised: 22 September 2023 and 29 September 2023 | Accepted: 2 October 2023

 DOI: https://doi.org/10.48084/etasr.6359

ABSTRACT

This paper presents an analytical model for computing and designing a three-phase Amorphous Core Transformer (ACT) with a power rating of 3 kVA, 380/127 V. Based on the main parameters obtained from the analytical model, a Finite Element Method (FEM) was developed to simulate the electromagnetic parameters, such as electric currents, operating voltages, and losses. Finally, an ACT installation was carried out with the steel material of code 2605SA1. The simulation results were compared with the experimental measurements under no-load and full-load operating conditions. Furthermore, the no-load loss of ACT was also compared to that of traditional transformers using silicon steel material. The obtained results prove that the use of ACT can save energy in the fields of education, health services, and industries.

Keywords-amorphous core transformer; current; no load; full load; finite element method

I. INTRODUCTION

The Amorphous Core Transformer (ACT) was first produced in the 1980s and was initially used as the steel core for electrical devices operating at high frequencies in the KHz range. However, later, it found applications as the steel core for industrial-frequency transformers. ACTs have special microstructural and compositional characteristics that reduce core losses: very low magnetic impedance (HC ≈ 5-10 A/m compared to ~50-100 A/m for silicon steel), thin thickness of steel laminations (td ≈ 0.03mm compared to ~0.3-0.5 mm for silicon steel), and very high resistivity (ρ ≈ 130-170 μΩcm compared to ~50-60 μΩcm for silicon steel). These properties significantly reduce core losses in amorphous steel compared to best-quality silicon steel [1-2]. Currently, researchers and transformer manufacturers have constantly explored new materials, modified designs, and improved manufacturing technologies to enhance structure, shape, technical specifications economics, and reduce the no-load losses of transformers, such as eddy currents and hysteresis effects in the steel core [3]. The hysteresis loss depends on the material quality, while the eddy current loss depends on the thickness of the lamination stack. The no-load loss is a continuous loss throughout the operation of the transformer. As a result, the no-load loss constitutes a significant portion of the total losses in the transformer. Manufacturers are always looking for ways to minimize transformer losses while also improving operational reliability [4]. Due to the unique core structure and rectangular winding of an ACT, the distribution of the electric field and the force acting on the winding will vary along the same coil. This distinction becomes more prominent during short-circuit events, which pose a significant danger to the winding [5]. The electromagnetic force exerted on the transformer winding arises from the interaction between the current and magnetic field in the windings. When the transformer operates under normal conditions, the influence of electromagnetic forces on the smaller winding is relatively minor due to the small magnetic field. However, during a short-circuit event, when the current in the winding and the magnetic flux increase significantly, a substantial electromagnetic force acts upon the winding. Among all transformer faults, winding-related issues account for 33% of the total, and these faults stem from short circuits: between turns of the High Voltage (HV) winding or Low Voltage (LV) winding, between different layers of winding, between HV and LV windings, and between phases in the same winding. These circumstances generate mechanical forces that can bend or damage the transformer winding [6-8].

In [5], the 2D Finite Element Method (FEM) was used to analyze and calculate the magnetic field of a 160 KVA ACT, considering the model in a short-circuit mode with maximum current. This study did not design an ACT model and did not

consider the 3D model under various operating conditions, such as no-load and rated load. In [9], the electromagnetic transients of a 25 KVA 3-phase oil-filled distribution transformer were analyzed using Ansys Maxwell simulation software. The simulation results provided values for losses, voltages, currents, and magnetic flux in the designed transformer, while the input voltage results aligned with the provided excitation values. Critical points on the core are discernible from the distribution of magnetic flux. The accuracy of the magnetic flux findings in this study was affirmed by comparison with similar studies. In [10], FEM was used to construct an analytical model for a 3-phase 50 MVA – 110/22 KV power transformer and to assess the impact of short-circuit impedance on the cumulative electromagnetic force effect. This study also involved subjecting the model to short-circuit current conditions to investigate the electromagnetic forces exerted on the transformer windings. In [11], a new model was developed to treat a 2D stress distribution problem, determining the stress distribution in the winding by solving the relevant equations. This study focused on the LV winding of a 110 KV transformer, which consisted of two continuously transposed conductors connected in parallel within a single disk, resulting in a model comprising two copper layers and one paper layer. Both the hoop stress and the radial stress distributions were calculated, and the obtained results were validated by FEM. Studies in [12-21] used FEM to analyze and compute the distribution of magnetic fields, impedance, and electromagnetic forces acting on the HV and LV windings of transformers during short-circuit operation. These studies provided formulas to calculate short-circuit currents and transient electromagnetic forces. In general, these studies provided results related to electrical losses, calculations, designs, and simulations focusing primarily on 22/0.4 KV distribution transformers. However, so far, there have been no specific studies on the design, experimentation, and simulation of lower-capacity ACTs with lower voltage levels.

This study used the analytic approach and FEM to calculate and design an ACT with small power capacity, commonly used as voltage stabilizers, power sources, or voltage converters in residential settings, educational institutions, small industries, industrial parks, and factories. The results obtained from the simulation were compared with measured results to validate the development of the proposed method. Based on the results obtained, it is possible to provide technical recommendations for the design, testing, and operation of ACTs.

II. ANALYTIC THEORY

A. Calculation of the Magnetic Circuit

The practical test was a 3-phase 3 KVA ACT, with primary and secondary voltages of 380/127 V, and a vector group of Y/Y_n. Figure 1 shows the structure of the ACT. The capacity power (S_t) for each core is defined as $S_t = S_{rated}/3$. This power depends on the material properties made of the iron core. Thus, the approximate formulation to define the cross-sectional area (T) of the iron core is [22-24]:

$$T = 2 \times c \times d = 4200 \text{ mm}^2 \quad (1)$$

where the magnetic flux density in the magnetic circuit is B_t = 1, and c and d are the thickness and depth of the steel core.

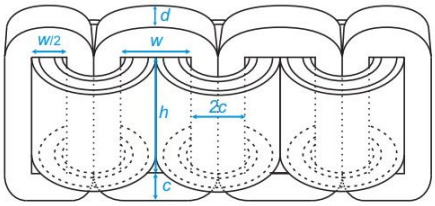

Fig. 1. Structure of ACT: d= 70 mm, c= 30 mm, h= 100 mm, w= 50 mm.

B. Computation of Windings

The turn numbers of the HV winding N_1 and LV winding N_2 are defined through the turn number winding per volt n_v as:

$$n_v = \frac{10^6}{4.44 \times B_t \times T \times f} = \frac{10^6}{4.44 \times 1 \times 4200 \times 50} = 1.1 \quad (2)$$

Equation (2) gives N_1 = 250 turns and N_2 = 83 turns. By selecting the current density J = 5 A/mm^2, the general winding diameter is calculated as:

$$d = 2\sqrt{\frac{I}{\pi . J}} \quad (3)$$

From (3), the diameter d_1 and the cross-section s_1 of the HV winding can be obtained as:

$$d_1 = 0.4\sqrt{I_{1p}} = 0.4\sqrt{4.56} = 0.9 \text{ mm}$$

$$s_1 = \left(\frac{d_1}{2}\right)^2 . \pi = \left(\frac{0.8}{2}\right)^2 . \pi = 0.5 \text{ mm}^2$$

Similarly, the diameter d_2 and the cross-section s_2 of the LV winding can be obtained as: d_2 = 1.2 mm and s_2 = 1.1 mm^2. The layer number of electrical insulation m_1 of the HV winding is defined as:

$$m_1 = \frac{N_1}{n_1} = \frac{250}{100} = 2.5 \quad (4)$$

The width Δ_1 of the HV winding is defined as:

$$\Delta_1 = m_1(d_1 + \gamma_1) = 3(0.8 + 2) = 8.4 \text{ mm} \quad (5)$$

where γ_1 is the thickness of the electrical insulation of the winding (γ_1 = 2 mm), m_1 = 3 layers, and Δ_1 = 10 mm instead of Δ_1 = 8.4 mm given in (5). In the same way, the thickness of the LV winding Δ_2 is:

$$\Delta_2 = m_2(d_2 + \gamma_2) = 2(1.2 + 2) = 6.4 \text{ mm} \quad (6)$$

where γ_2 is also the thickness of electrical insulation of the winding (γ_2 = 2 mm), m_2 = 3 layers, and Δ_2 = 8 mm instead of Δ_2 = 6.4 mm given in (6). The width of the magnetic circuit window can be computed as:

$$w = 2\delta_0 + 2\delta_{12} + \delta_3 + 2\Delta_1 + 2\Delta_2$$
$$= 2.2 + 2.1 + 5 + 2.10 + 2.8 = 47 \text{ mm} \quad (7)$$

In general, the width of the magnetic circuit window is chosen bigger than 20-30% due to the winding layers being not flat [24]. Thus, w = 50 mm. Finally, the cross-section area S_c is defined as:

$$S_c = h \times w = 100 \times 50 \text{ mm}^2 \quad (8)$$

Figure 2 shows all the design parameters. The basic electrical parameters and the design dimensions of the 3-phase 3 KVA-380/127 V ACT are also listed in Table I. Figure 3 illustrates the process of calculation, comparison, and development of the comprehensive simulation model from the initial design to the final results of this study.

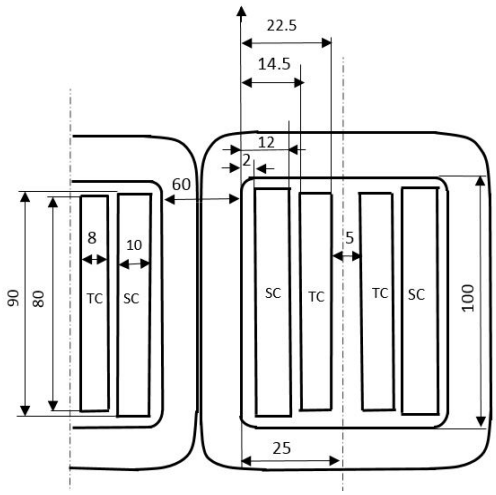

Fig. 2. Cross-section structure of the ACT.

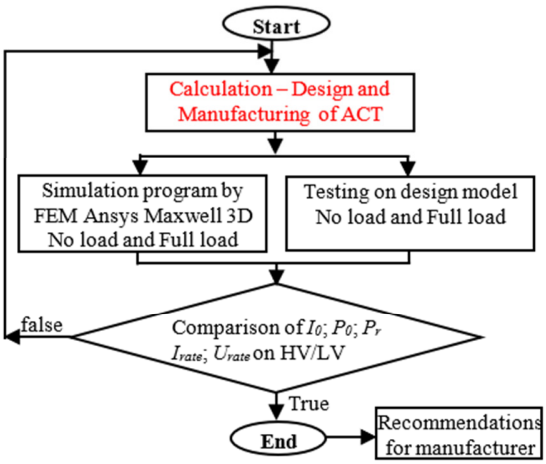

Fig. 3. Process of calculation of the ACT.

TABLE I. BASIC PARAMETERS OF THE ACT

No	Parameter	Value
1	Phase number	3
2	Frequency [Hz]	50
3	Rated power [kVA]	3
4	Wiring connection	Y/Y
5	Voltage of HV/LV [V]	380/127
6	No. of turns of HV/LV windings	250/83
7	Phase current of HV/LV windings [A]	4.56/13.64
8	Winding diameter d_1/d_2 [V]	0.8/1.2
9	Electric current density J [A/mm^2]	5
10	Core thickness c [mm]	30
11	Width of core window w [mm]	50
12	Height of magnetic circuit window h [mm]	100

III. FINITE ELEMENT APPROACH

The ANSYS Maxwell tool (V19.R1) was used to calculate and simulate the electromagnetic parameters of the ACT [26]. Figure 4 shows the geometry of the 3 kVA-380/127V 3D-ACT. The problem was solved with different scenarios, including no-load, rated load, and short-circuit conditions.

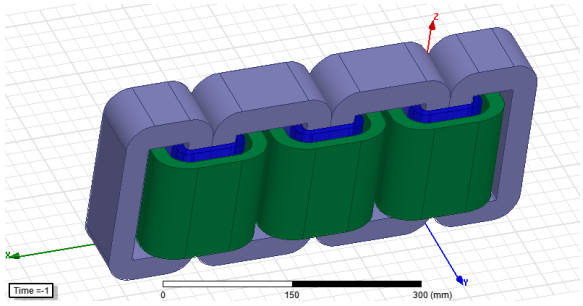

Fig. 4. Amorphous Transformer in Ansys Maxwell 3D

A. *No-Load Operation*

Figure 5 illustrates the distribution of magnetic flux density in the magnetic circuit. It can be observed that most of the magnetic flux was concentrated in the magnetic circuit without in the air. The maximum value was 1.57 T. As a result, the leakage magnetic flux on the HV and LV windings was very small and nearly zero. Figures 6 and 7 show the waveforms of the HV and LV windings, respectively.

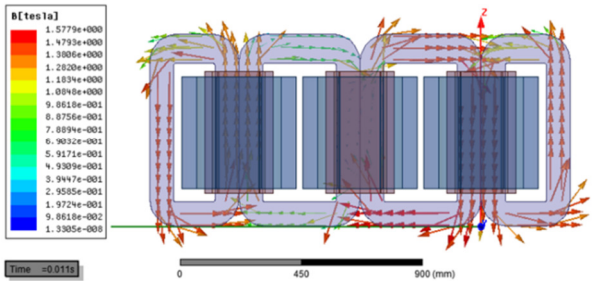

Fig. 5. Magnetic flux density distribution due to the 3-phase currents.

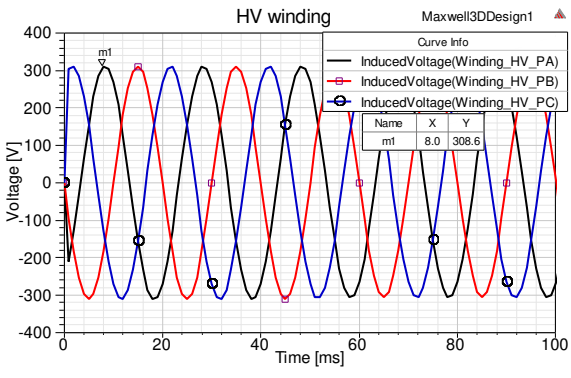

Fig. 6. Waveform of the HV winding.

In Figure 6, the simulation results indicate an effective phase voltage value of 218 V for the HV winding, compared to

the calculated phase voltage value of 220 V. Similarly, in Figure 7, the effective phase voltage value for LV was 72.4 V, compared to the calculated phase voltage of 73 V. For the no-load operation, the electric current in the LV winding was equal to zero. However, the no-load current in the HV winding was different from zero and is shown in Figure 8. It can be seen that the no-load phase current of the HV winding was 0.036 A. Figure 9 presents the joule losses for the no-load and full-load operations. The steady-state no-load loss value reached 10.5 W.

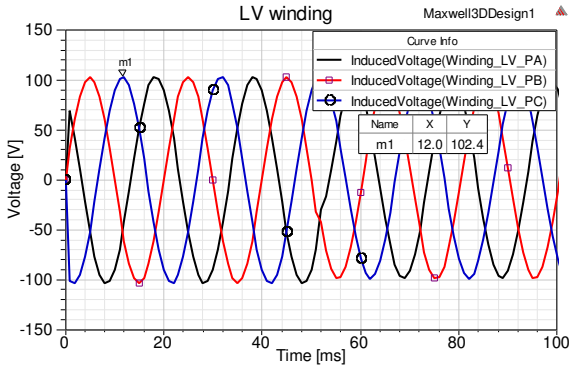

Fig. 7. Waveform of the LV winding.

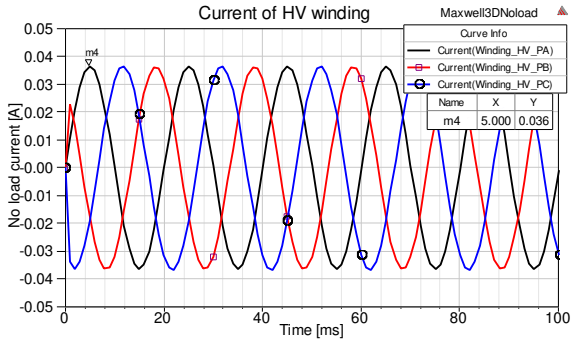

Fig. 8. No-load current in the HV winding.

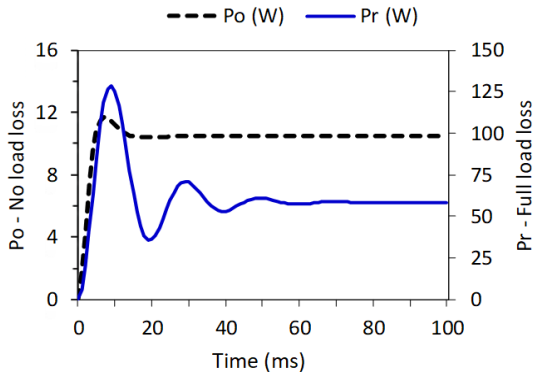

Fig. 9. Joule losses for no-load and full-load operations.

B. Full-Load Operation

Figures 10 and 11 show the distribution of the currents in the HV and LV windings, respectively.

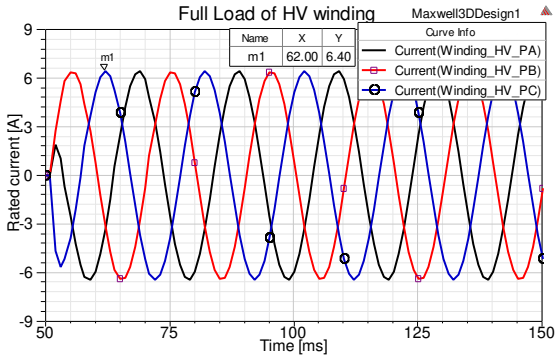

Fig. 10. Rated currents in the HV winding.

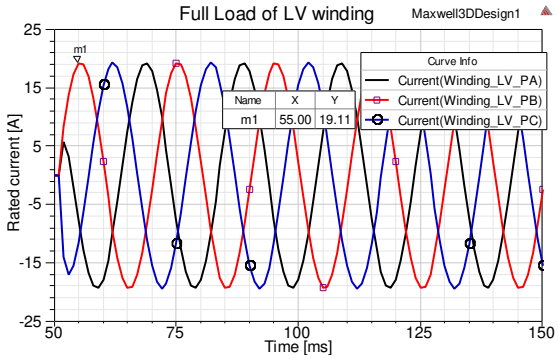

Fig. 11. Rated currents in the LV winding.

Figure 10 shows that the simulated current in the HV winding was 4.53 A compared to the analytic current of 4.56 A. In the same way, Figure 11 shows that the value of the rated current in the LV winding was 13.51 A compared to the analytic current of 13.64 A. The rated loss reached 58.2 W.

IV. ACT MANUFACTURING AND ASSEMBLING

A. Manufacturing the Magnetic Circuit of ACT

A 3-phase 3 KVA 380/127 V ACT was assembled, as shown in Figures 12 and 13. The turn numbers of the HV and LV windings were $W_1 = 250$ and $W_2 = 83$ turns, respectively.

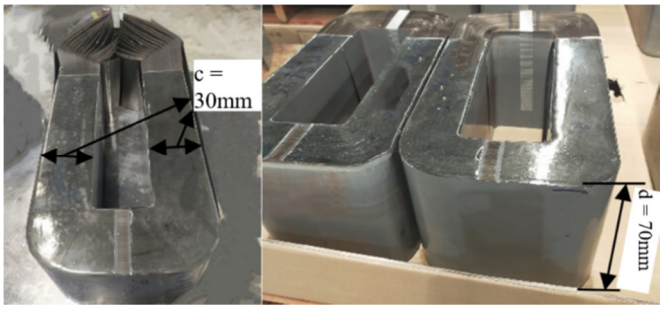

Fig. 12. Magnetic circuit assembling.

B. Diagram of No-Load and Rated-Load Experiments

Figure 14 shows the diagram of the no-load and rated load experiments [23-25]. First, the no-load operation was carried out to measure the values of no-load current, voltage, and joule loss.

Fig. 13. Completing the manufacture of ACT.

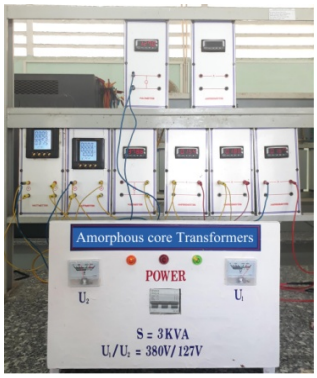

Fig. 14. Diagram of no-load and rated load experiments.

Then, the rated load experiment was carried out to measure the rated current and loss. Three 3kVA 380/127 V transformers were used to experimentally measure their no-load current and no-load loss: (1) SCT_1: Silicon core Transformer 1, (2) SCT_2: Silicon Core Transformer 2, and (3) the designed ACT. A comparison was carried out to determine the loss reduction capacity of the ACT design, as shown in Table II. From the results of Table II, it can be seen that the designed ACT had losses reduced by 75% compared to the SCT.

TABLE II. COMPARISON OF NO-LOAD LOSS OF TRANSFORMERS

Parameter	SCT_1 [25]	SCT_2 [25]	Design ACT
No load loss P_0(W)	48	42	11
No load current I_0 (A)	0.26	0.20	0.045
Rated current of HV winding I_{rate_HV} (A)	4.6	4.6	4.56
Rate no load i_0%	5.4%	4.1%	1%

C. Experimental Results

After carrying out the no-load and rated-load experiments, the results of currents, voltages, and joule losses were measured as given in Table III. It can be seen that the simulated values were smaller than the experimental values because the simulation did not take into account the characteristics of eddy currents, insulation materials, and the support structure of the transformers. Specifically, these errors fluctuated within the range of 2.2-5.9%. In particular, the error for the no-load current value was 25%. This substantial error arises because the no-load current value is very small and this error is influenced by the measurement equipment.

TABLE III. COMPARISON OF THE SIMULATED AND MEASURED RESULTS

No	Parameter	Simulated results	Measured results	Errors (%)
1	No load current I_0 (A)	0.036	0.045	25
2	$I_{rate\text{-}HV}$ (A) of HV winding	4.53	4.80	5.9
3	$I_{rate\text{-}LV}$ (A) of LV winding	13.51	14.2	5.1
4	U_{1HV} (V) of HV winding	218	225	3.2
5	U_{1LV} (V) of LV winding	72.4	74	2.2
6	No load loss P_0 (W)	10.5	11.0	4.7
7	Full load loss P_r (W)	58.2	61.5	5.6

V. CONCLUSION

This study involved the calculation, design, and production of a 3-phase 3 KVA 380/127V ACT. In addition to the analytical method, FEM and an experimental method were carried out under both no-load and rated-load conditions. The simulated results for the rated voltage, current, and no-load and rated-load losses were compared and evaluated against the experimental data. The error assessment displayed an oscillation range of 2.2-5.9%, indicating that the accuracy between the two methods is nearly equivalent. This study also successfully designed and manufactured a 3-phase 3 KVA, 380/127V ACT to experimentally prove the ability to reduce the no-load losses of this design. This study opens up new possibilities to design and manufacture energy-efficient transformers, not only for high power but also for smaller capacities and lower voltage levels. These results can serve as experimental models and educational tools for universities and research institutions.

ACKNOWLEDGMENT

This work was supported by the project B2022-DQN-03 sponsored by the Ministry of Education and Training, Vietnam.

REFERENCES

[1] M. A. Bahmani, "Core Loss Calculation in Amorphous High Frequency High-Power Transformers with Different Topologies," MSc Thesis, Chalmers University Of Technology Gothenburg, Sweden, 2011.

[2] L. Roginskaya, Z. Yalalova, A. Gorbunov, and J. Rakhmanova, "Features of amorphous steel magnetic cores for transformers operating at mains frequency," in *2020 International Conference on Electrotechnical Complexes and Systems (ICOECS)*, Ufa, Russia, Jul. 2020, pp. 1–5, https://doi.org/10.1109/ICOECS50468.2020.9278451.

[3] M. Nazmunnahar, S. Simizu, P. R. Ohodnicki, S. Bhattacharya, and M. E. McHenry, "Finite-Element Analysis Modeling of High-Frequency Single-Phase Transformers Enabled by Metal Amorphous Nanocomposites and Calculation of Leakage Inductance for Different Winding Topologies," *IEEE Transactions on Magnetics*, vol. 55, no. 7, pp. 1–11, Jul. 2019, https://doi.org/10.1109/TMAG.2019.2904007.

[4] C.-H. Hsu, C.-Y. Lee, Y.-H. Chang, F.-J. Lin, C.-M. Fu, and J.-G. Lin, "Effect of Magnetostriction on the Core Loss, Noise, and Vibration of Fluxgate Sensor Composed of Amorphous Materials," *IEEE Transactions on Magnetics*, vol. 49, no. 7, pp. 3862–3865, Jul. 2013, https://doi.org/10.1109/TMAG.2013.2248702.

[5] T.-H. Le, D. D. Tung, and B. D. Thanh, "Computation of electromagnetic forces in the windings of amorphous core transformers," *Archives of Electrical Engineering*, vol. 72, no. 2, pp. 521–539, 2023, https://doi.org/10.24425/aee.2023.145423.

[6] A. H. Z. Bkhaitawi, A. A. Abdoos, and A. Ebadi, "Presenting an Adaptive Restraint Method to Improve Performance of Ground Differential Protection of Power Transformer," *International Journal of*

Engineering, vol. 35, no. 11, pp. 2213–2219, Nov. 2022, https://doi.org/10.5829/ije.2022.35.11b.16.

[7] A. Yahiou, H. Mellah, and A. Bayadi, "Inrush Current Reduction by a Point-on-wave Energization Strategy and Sequential Phase Shifting in Three-Phase Transformer," *International Journal of Engineering*, vol. 35, no. 12, pp. 2321–2328, Dec. 2022, https://doi.org/10.5829/ije.2022.35.12c.07.

[8] H. M. Ahn, Y. H. Oh, J. K. Kim, J. S. Song, and S. C. Hahn, "Experimental Verification and Finite Element Analysis of Short-Circuit Electromagnetic Force for Dry-Type Transformer," *IEEE Transactions on Magnetics*, vol. 48, no. 2, pp. 819–822, Oct. 2012, https://doi.org/10.1109/TMAG.2011.2174212.

[9] S. Bal, T. Demirdelen, and M. Tümay, "Three-Phase Distribution Transformer Modeling and Electromagnetic Transient Analysis Using ANSYS Maxwell," in *2019 3rd International Symposium on Multidisciplinary Studies and Innovative Technologies (ISMSIT)*, Ankara, Turkey, Jul. 2019, pp. 1–4, https://doi.org/10.1109/ISMSIT.2019.8932953.

[10] Y. Li, Q. Xu, and Y. Lu, "Electromagnetic Force Analysis of a Power Transformer Under the Short-Circuit Condition," *IEEE Transactions on Applied Superconductivity*, vol. 31, no. 8, pp. 1–3, Aug. 2021, https://doi.org/10.1109/TASC.2021.3107799.

[11] M. Jin *et al.*, "Stress Distribution Characteristics of Composite Wire-Paper Winding Structure under the Radial Electromagnetic Force," in *2021 IEEE Electrical Insulation Conference (EIC)*, Denver, CO, USA, Jun. 2021, pp. 597–601, https://doi.org/10.1109/EIC49891.2021.9612347.

[12] Y. Zhai, R. Zhu, Q. Li, X. Wang, Y. Gu, and S. Li, "Simulation Research on Electrodynamic Force and Deformation of Transformer Windings under Short-circuit Condition," in *2022 IEEE International Conference on High Voltage Engineering and Applications (ICHVE)*, Chongqing, China, Sep. 2022, pp. 1–4, https://doi.org/10.1109/ICHVE53725.2022.9961358.

[13] Y. Zhao, T. Wen, Y. Li, H. Ni, Q. Zhang, and W. Chen, "A FEM-based simulation of electromagnetic forces on transformer windings under short-circuit," in *2018 IEEE International Power Modulator and High Voltage Conference (IPMHVC)*, Jackson, WY, USA, Jun. 2018, pp. 425–429, https://doi.org/10.1109/IPMHVC.2018.8936726.

[14] K. Dawood, G. Komurgoz, and F. Isik, "Computation of the Axial and Radial forces in the Windings of the Power Transformer," in *2019 4th International Conference on Power Electronics and their Applications (ICPEA)*, Elazig, Turkey, Sep. 2019, pp. 1–6, https://doi.org/10.1109/ICPEA1.2019.8911132.

[15] M. Jin *et al.*, "Influence of Frequency Components of Short-Circuit Electromagnetic Force on Vibration Characteristics of Power Transformer Windings," in *2022 IEEE International Conference on High Voltage Engineering and Applications (ICHVE)*, Chongqing, China, Sep. 2022, pp. 01–04, https://doi.org/10.1109/ICHVE53725.2022.9961671.

[16] K. Dawood and G. Komurgoz, "Investigating effect of Electromagnetic Force on Sandwich Winding Transformer using Finite Element Analysis," in *2021 28th International Workshop on Electric Drives: Improving Reliability of Electric Drives (IWED)*, Moscow, Russia, Jan. 2021, pp. 1–5, https://doi.org/10.1109/IWED52055.2021.9376371.

[17] J. U. Kothavade and P. Kundu, "Investigation Of Electromagnetic Forces In Converter Transformer," in *2021 IEEE 2nd International Conference on Smart Technologies for Power, Energy and Control (STPEC)*, Bilaspur, Chhattisgarh, India, Sep. 2021, pp. 1–6, https://doi.org/10.1109/STPEC52385.2021.9718676.

[18] Y. Zhao *et al.*, "Short-Circuit Electromagnetic Force Distribution Characteristics in Transformer Winding Transposition Structures," *IEEE Transactions on Magnetics*, vol. 56, no. 12, pp. 1–8, Sep. 2020, https://doi.org/10.1109/TMAG.2020.3028832.

[19] A. Yahiou, H. Mellah, A. Bayadi, and M. Abid, "Effects of Inrush Current on the Hysteresis Loop and Load Influences on the Transient Current of a Single-Phase Transformer," *Engineering, Technology & Applied Science Research*, vol. 12, no. 5, pp. 9258–9264, Oct. 2022, https://doi.org/10.48084/etasr.5205.

[20] V. D. Quoc, "Accurate Magnetic Shell Approximations with Magnetostatic Finite Element Formulations by a Subdomain Approach," *Engineering, Technology & Applied Science Research*, vol. 10, no. 4, pp. 5953–5957, Aug. 2020, https://doi.org/10.48084/etasr.3678.

[21] V. D. Quoc, "Robust Correction Procedure for Accurate Thin Shell Models via a Perturbation Technique," *Engineering, Technology & Applied Science Research*, vol. 10, no. 3, pp. 5832–5836, Jun. 2020, https://doi.org/10.48084/etasr.3615.

[22] O. Taylor, J. Overmyer, and R. Michaelis, *Transformer Principles and Applications*. Homewood, IL, USA: American Technical Publishers, 2006.

[23] J. H. Harlow, *Electric Power Transformer Engineering*. Boca Raton, FL, USA: CRC Press, 2003.

[24] B. P. Van and D. L. Van, *Transformer Design*. Hanoi, Vietnam: Science & Technology Publishing Company, 2011.

[25] G. Ala *et al.*, "Stability of Microgrids: An Application of Virtual Synchronous Generator," in *Advances in Engineering Research and Application*, 2023, pp. 873–880, https://doi.org/10.1007/978-3-031-22200-9_92.

[26] "Ansys Maxwell | Electromechanical Device Analysis Software." https://www.ansys.com/products/electronics/ansys-maxwell.